6. Oscillatory stability and RE

History of oscillαtory stability analysis

Power swing seems to occur more frequently than voltage collapse or asynchronism, the author experienced twice in his duty of electric engineer. The first occurred in 1981; power swing with 2 sec. period lasted, and signal at knight downtown was reported flickered. Recording system in those days ware so poor that no data exist here to be introduced. To clarify the phenomenon, the author was converted from distribution section to power system section. Because, the phenomenon was nor reproduced by simulation tool that was introduced just before the phenomenon. Investigation clarified that data were not adequate. Gathering generator, excitation system, speed governing system, the phenomenon was almost reproduced. But power swing became slightly growing than reality. Then, by giving 1 p.u. danping at shaft, the phenomenon was successfully reproduced. Later a colleague introduced load's frequency sensitivity as damping, shaft damping was replaced to 2 p.u. frequency sensitivity of load, because power swing occurs generators and infinite bus, so frequency swing as load is almost half at shaft.

The second occurred in 1985 also 2 sec. period power swing(1)(2). Since good record system was already adopted, the record was reported in repository, thus Fig. 6.1 survives. To tell the truth the author predicted the phenomenon. In thermal generator quadrature axis transient component (Xq' and Tq') should be considered, deduced from damp test record. Considering the quadrature axis transient component, variation of generator voltage is reproduced better. However, considering the component, generator's damping effect is reduced, and power swing become occur more easily. By simulation, it was found that stability limit power flow at one-circuit tie line is reduced to 200MW, while that was 400MW in operation manual that was made without considering the component. There was a negative margin. The author of course warned, but superior neglected. Soon, really power swing occurred at two-circuit tie line with 180MW sending power flow. Prediction by the author was proved. Superior of superior and further superior became very angry of course, and PSS was equipped in thermal generators as soon as possible. Thereafter in the utility the author contributed, quadrature axis transient component has been considered in thermal generators, but many other utilities still neglect that and are assessing oscillatory stability optimistically.

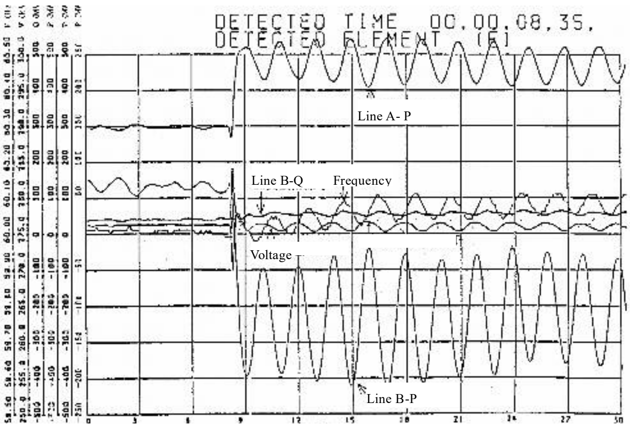

Fig. 6.1 Power swing observed in 1985

By the way, in 1982 of the convert, the reason why the author succeeded to reproduce power swing is, of course, history of oscillatory stability research. The oldest contribution was made by Heffron and Phillips(3), which is refered in Ref. (4) that the author already red. But it dealt rather intending to extend leading power factor operational region. It was Demello and Concordia(5) in 1969 that first focused relationship between power swing and excitation system design. However until then, one machine infinite bus model was used. The model is realistic in case that far large power source send power via long line to power pool, but is not realistic in case that large interconnection is divided into two groups and they swing each other, and it is impossible to deal with impacts by load model, aggregation, and RE. Komami and Komukai(6)(7) in 1987 extended Demello-Concordia by modeling midway load having voltage sensitivity. Yamagishi and Komami[(8)] in 2006 further extended by assessing impact by highly integrated RE. Komami, Sakata, and Yamada[(9)] in 2016 further extended by quantitatively assessing harmful side effect of RE's frequency feedback type anti-islanding on oscillatory stability.

Since contents of the chapter is based on Komami-Komukai theory, it is explained. Fundamental equations of synchronous machine to elegantly solve oscillatory stability by manual calculation are written in Kimbark(10). In the last stage block diagram is given. Block diagram clearly express input and output, they are correspond cause and result, therefore, is more strict expression than others, and once expressed in the form analysis is half finished. However, to minutely state process toward block diagram scientific paper has limitation of pages, so reference is much used, thus the situation that any engineer don't know the theory (such world is called as "Meppo" in Buddhism). So in ref. (9),all process are written in paper itself so that younger engineers can read (such world is called in Mappo in Buddhism as slightly better world than Meppo) .

Komami-Komukai theory[(9)]

System model considering midway load on one machine infinite bus system is the minimum model for oscillatory stability analysis. Its structure is shown in Fig. 6,2. All paths from trunk bus to internal load are considered.

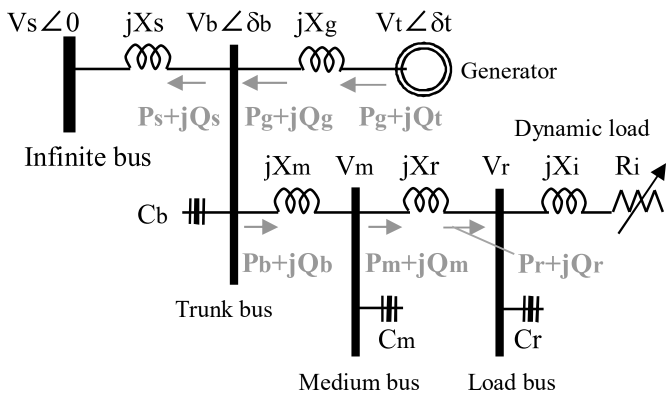

Fig. 6.2 Minimum model for oscillatory stability analysis

Initial power flow condition Oscillatory stability deals with relationship among little deviations around equilibrium. Load's voltage sensitivity seen from trunk bus much affects to whole system character. The sensitivity differs in stationery condition and transient condition by the nature of motor. In the theory the voltage sensitivity is dealt as parameter.

Character under the trunk bus (Vb) is dealt afterward. Flow in trunk system can be expressed by voltages and angles of nodes as follows.

$$\left.\begin{aligned} Ps &= \frac{Vb\ Vs \sin\delta b}{Xs} & Qs &= \frac{Vb^2 - Vb\ Vs\cos\delta b}{Xs} \\ Pg &= \frac{Vt\ Vb\sin(\delta t-\delta b)}{Xg} & Qg &= \frac{Vt\ Vb\cos(\delta t-\delta b) - Vb^2}{Xg} \\ & & Qt &= \frac{Vt^2 - Vt\ Vb\cos(\delta t-\delta b)}{Xg} \end{aligned}\right\} \quad (6.2)$$

Small deviations around equilibrium of eq. (6.2) are expressed as follows.

$$\left.\begin{aligned} \varDelta Ps &= Ps\frac{\varDelta Vb}{Vb} - \left(Qs - \frac{Vb^2}{Xs}\right)\varDelta\delta b \qquad \varDelta Qs = \left(Qs + \frac{Vb^2}{Xs}\right)\frac{\varDelta Vb}{Vb} + Ps\,\varDelta\delta b \\ \varDelta Pg &= Pg\frac{\varDelta Vt}{Vt} + Pg\frac{\varDelta Vb}{Vb} + \left(Qg + \frac{Vb^2}{Xg}\right)(\varDelta\delta t - \varDelta\delta b) \end{aligned}\right\} \quad (6.3)$$

$$\left.\begin{aligned}\varDelta Qg &= (Qg + \frac{Vb^2}{Xg})\ \frac{\varDelta Vt}{Vt}\ + (Qg - \frac{Vb^2}{Xg})\ \frac{\varDelta Vb}{Vb}\ - Pg\,(\varDelta\delta t - \varDelta\delta b)\\ \varDelta Qt &= (Qt + \frac{Vt^2}{Xg})\ \frac{\varDelta Vt}{Vt}\ + (Qt - \frac{Vt^2}{Xg})\ \frac{\varDelta Vb}{Vb}\ + Pg\,(\varDelta\delta t - \varDelta\delta b)\end{aligned}\right\}$$

Load's character seen from trunk bus is assumed as index function that active power is proportional V^{α}, reactive power is proportional to V^{β}, capacitor/reactor reactive power is proportional to V^{γ}. Here, Qcb is reactive power generated by capacitor Cb.

$$\varDelta Pb = \alpha\ Pb\ \frac{\varDelta Vb}{Vb}\ ,\quad \varDelta Qb = \beta\ Qb\ \frac{\varDelta Vb}{Vb}\ ,\quad \varDelta Qcb = \gamma\ Qcb\ \frac{\varDelta Vb}{Vb} \tag{6.4}$$

Balance of flows' small deviation is expressed as follows.

$$\varDelta Pg = \varDelta Pb + \varDelta Ps\ ,\quad \varDelta Qg + \varDelta Qcb = \varDelta Qb + \varDelta Qs \tag{6.5}$$

By eq. (6.3), (6.4), (6.5), not important variables $\varDelta\delta b$ and $\varDelta Vb/Vb$ can be expressed by important variables $\varDelta\delta t$ and $\varDelta Vt/Vt$. Of course using the relationship not important variables $\varDelta\delta b$ and $\varDelta Vb/Vb$ are put away.

$$\begin{pmatrix}\varDelta\delta b\\ \frac{\varDelta Vb}{Vb}\end{pmatrix} = \begin{pmatrix}A_{11} & A_{12}\\ A_{21} & A_{22}\end{pmatrix}\begin{pmatrix}\varDelta\delta\\ \frac{\varDelta Vt}{Vt}\end{pmatrix} \tag{6.6}$$

Substituting eq. (6.6) to equations of $\varDelta Pg$ and $\varDelta Qt$ in eq. (6.3), not important variables $\varDelta\delta b$ and $\varDelta Vb/Vb$ are put away, relationship as follows is obtained.

$$\begin{pmatrix}\varDelta Pg\\ \varDelta Qt\end{pmatrix} = \begin{pmatrix}Pg_1 & Pg_2\\ Qt_1 & Qt_2\end{pmatrix}\begin{pmatrix}\varDelta\delta t\\ \frac{\varDelta Vt}{Vt}\end{pmatrix} \tag{6.7}$$

Fundamental equations of synchronous machine　　Those are expressed as follows[4].

$$\left.\begin{aligned}&\mathbf{V_t} = Vd + j\,Vq \qquad \mathbf{I} = Id + j\,Iq \qquad \Psi = \Psi d + j\,\Psi q\\ &Vd = s\,\Psi d - \Psi q\,s\,\theta \qquad Vq = s\,\Psi q + \Psi q\,s\,\theta\\ &\Psi d = If - Xd\,Id \qquad \Psi q = -\,Xq\,Iq\\ &\Psi fd = If - (Xd - Xd')\,Id \qquad Efd = If + Tdo'\,s\,\Psi fd\\ &\frac{(M\,s^2 + D\,s)\,\delta}{\omega_0} = Tm - Te \qquad Te = \Psi d\,Iq - \Psi q\,Id\ \fallingdotseq\ Pg\end{aligned}\right\} \tag{6.8}$$

Here, nomenclature is explained.

Vt : terminal voltage,　 Vd :　: its direct axis component,　 Vq : its quadrature axis component,

I : generator current,　 Id : its direct axis component,　 Iq : its quadrature axis component,

Ψ : armature flux linkage,　 Ψd : its direct axis component,　 Ψq : its quadrature axis component,

s : Laplace transform.　 θ : rotor position,　 δ : rotor phase angle,

If : field current,　 Ψfd : field flux linkage,　 Efd : field voltage

X_d : direct axis synchronous reactance, X_q : quadrature axis synchronous reactance,

X_d' : direct axis transient reactance, T_{do}' : direct axis open transient time constant (sec.),

M : unit inertia constant (sec.), D : Damping coefficient, ω_0 : system angle frequency,

T_m : mechanical input torque, Te : electric output torque

Electric output power Pg is product of torque Te and speed n, but speed deviation is very small, it is practically reasonable to recognize as Te = Pg.

Vector diagram of operating generator is expressed as Fig. 6.3(2). Equation as follows are derived from vector diagram.

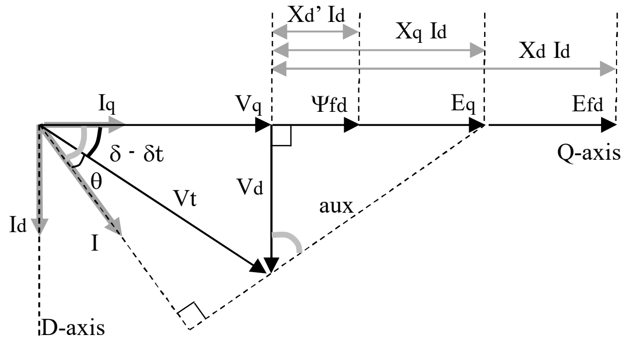

Fig. 6.3 Vector diagram of synchronous machine

$$\left.\begin{aligned}
E_q &= \{(V_t + X_q\frac{Q_t}{V_t})^2 + (X_q\frac{P_g}{V_t})^2\}^{1/2} \\
\sin(\delta - \delta_t) &= \frac{X_q P_g}{E_q V_t} \\
P_g + j Q_t &= \mathbf{V_t I^*} = (V_d I_d + V_q I_q) + j(V_q I_d - V_d I_q) \\
I_d &= \frac{P_g \sin(\delta - \delta_t)}{V_t} + \frac{Q_t \cos(\delta - \delta_t)}{V_t} \\
I_q &= \frac{P_g \cos(\delta - \delta_t)}{V_t} - \frac{Q_t \sin(\delta - \delta_t)}{V_t} \\
V_d &= X_q I_q \\
V_q &= (V_t^2 - V_d^2)^{1/2} = \Psi_{fd} - X_d' I_d
\end{aligned}\right\} \quad (6.9)$$

Equation of E_q is understood by considering that Qt/Vt expresses reactive current Ireac and Pt/Vt does active current Iact.

Equation of I_d (by same way equation of I_q) is conducted, using power factor angle θ, from relations as follows.

$I_d = I\sin(\delta - \delta_t + \theta) = I\cos\theta \sin(\delta - \delta_t) + I\sin\theta \cos(\delta - \delta_t)$,

$I\cos\theta = P_g/V_t$, $I\sin\theta = Q_t/V_t$

Equation of V_d is understood by theory of similar figure considering that angle made by I and I_q is equal to that made by V_d and auxiliary line "aux".

Equation of $\sin(\delta - \delta_t)$ tells that generator can be expresses as voltage source E_q behind reactance X_q, vector **Eq** exists on Q axis. The equation is proven equivalent to real part of complex power:

$P_g = V_d I_d + V_q I_q$

which is directly conducted from definition of D and Q component of voltage and current:

$V_t = V_d + j V_q$, $I = I_d + j I_q$

Substituting these relationships as follows to active power equation,

$V_d = V_t \sin(\delta - \delta_t)$

$$Vd = Xq\ Iq \qquad \therefore \quad Iq = Vd / Xq$$

equation as follows is conducted.

$$Pg = Vd\ Id + Vq\ \frac{Vd}{Xq} = \frac{Vd\ (Xq\ Id + Vq)}{Xq} = \frac{Vt \sin(\delta - \delta t)\ (Xq\ Id + Vq)}{Xq} = \frac{Eq\ Vt \sin(\delta - \delta t)}{Xq}$$

Similar relationship exists in reactive power as follows.

$$Qt = Vq\ Id - Vd\ \frac{Vd}{Xq} = \frac{Vd\ Xq\ Id - Vt^2 + Vq^2}{Xq} = \frac{Vt \cos(\delta - \delta t)\ Xq\ Id - Vt^2 + Vq\ Vt \cos(\delta - \delta t)}{Xq}$$

$$= \frac{Eq\ Vt \cos(\delta - \delta t) - Vt^2}{Xq}$$

Small deviation of generator's voltage, active and reactive power in eq. (6.9) are expressed as follows.

$$\left.\begin{aligned}
&\Delta Vd = Xq\ \Delta Iq \\
&\Delta Vq = \Delta \Psi fd - Xd'\ \Delta Id \\
&\Delta Id = Id1\ \Delta\delta t + Id2\ \frac{\Delta Vb}{Vb} + Id3\ \Delta\delta \\
&\Delta Iq = Iq1\ \Delta\delta t + Iq2\ \frac{\Delta Vb}{Vb} + Iq3\ \Delta\delta \\
&\Delta Pg = Vd\ \Delta Id + Vq\ \Delta Iq + Id\ \Delta Vd + Iq\ \Delta Vq \\
&\Delta Qt = Vq\ \Delta Id - Vd\ \Delta Iq - Iq\ \Delta Vd + Id\ \Delta Vq
\end{aligned}\right\} \quad (6.10)$$

Coefficients in equations of currents' small deviation are expressed as follows using eq. (6.7).

$$Id1 = \frac{Pg1 \sin(\delta - \delta t) + Qt1 \cos(\delta - \delta t) - Pg \cos(\delta - \delta t) + Qt \sin(\delta - \delta t)}{Vt}$$

$$Id2 = \frac{Pg2 \sin(\delta - \delta t) + Qt2 \cos(\delta - \delta t) - Pg \sin(\delta - \delta t) - Qt \cos(\delta - \delta t)}{Vt}$$

$$Id3 = \frac{Pg \cos(\delta - \delta t) - Qt \sin(\delta - \delta t)}{Vt}$$

$$Iq1 = \frac{Pg1 \cos(\delta - \delta t) - Qt1 \sin(\delta - \delta t) + Pg \sin(\delta - \delta t) + Qt \cos(\delta - \delta t)}{Vt}$$

$$Iq2 = \frac{Pg2 \cos(\delta - \delta t) - Qt2 \sin(\delta - \delta t) - Pg \cos(\delta - \delta t) + Qt \sin(\delta - \delta t)}{Vt}$$

$$Iq3 = \frac{- Pg \sin(\delta - \delta t) - Qt \cos(\delta - \delta t)}{Vt}$$

Into equations of small deviation (6.10), substituting equations of voltage and current, and using eq. (6.7), relationship as follows is obtained.

$$\begin{pmatrix} B_{11} & B_{12} \\ B_{21} & B_{22} \end{pmatrix} \begin{pmatrix} \varDelta\delta t \\ \dfrac{\varDelta Vt}{Vt} \end{pmatrix} = \begin{pmatrix} B_{13} & B_{14} \\ B_{23} & B_{24} \end{pmatrix} \begin{pmatrix} \varDelta\delta \\ \varDelta\Psi fd \end{pmatrix}$$

Elements of the matrix are expressed as follows.

$$B_{11} = P_{g1} - V_d I_{d1} - V_q I_{q1} + I_q X_d' I_{d1} - I_d X_q I_{q1}$$

$$B_{12} = P_{g2} - V_d I_{d2} - V_q I_{q2} + I_q X_d' I_{d2} - I_d X_q I_{q2}$$

$$B_{13} = \quad V_d I_{d3} + V_q I_{q3} - I_q X_d' I_{d3} + I_d X_q I_{q3}$$

$$B_{14} = \quad I_q$$

$$B21 = Q_{t1} - V_q I_{d1} + V_d I_{q1} + I_d X_d' I_{d1} + I_q X_q I_{q1}$$

$$B_{22} = Qt2 - V_q I_{d2} + V_d I_{q2} + I_d X_d' I_{d2} + I_q X_q I_{q2}$$

$$B_{23} = \quad V_q I_{d3} - V_d I_{q3} - I_d X_d' I_{d3} - I_q X_q I_{d3}$$

$$B_{24} = \quad I_d$$

Transforming left side matrix to unit matrix by performing calculations only on rows, variables at terminal $\varDelta\delta t$ and $\varDelta Vt/Vt$ are expressed by variables internal generator $\varDelta\delta$ and $\varDelta\Psi fd$ as follows.

$$\begin{pmatrix} \varDelta\delta t \\ \dfrac{\varDelta Vt}{Vt} \end{pmatrix} = \begin{pmatrix} C_{13} & C_{14} \\ C_{23} & C_{24} \end{pmatrix} \begin{pmatrix} \varDelta\delta \\ \varDelta\Psi fd \end{pmatrix} \qquad (6.11)$$

Block diagram Substituting eq. (6.11) into eq. (6.7), relationship as follows is obtained.

$$\varDelta Pg = P_{g1} (C_{13}\ \varDelta\delta + C_{14}\ \varDelta\Psi fd) + P_{g2} (C_{23}\ \varDelta\delta + C_{24}\ \varDelta\Psi fd)$$

Therefore $\varDelta Pg = K_1\ \varDelta\delta + K_2\ \varDelta\Psi fd$ (6.12)

Here $K_1 = P_{g1} C_{13} + P_{g2} C_{23}$

$K_2 = P_{g1} C_{14} + P_{g2} C_{24}$

Erasing If from equation of Ψfd and E_{fd} of (6.8), relationship as follows is obtained.

$$(1 + T_{do}' s)\ \Psi fd = E_{fd} - (X_d - X_d')\ I_d$$

Small deviation of the equation is expressed as follows.

$$(1 + T_{do}' s)\ \varDelta\Psi fd = \varDelta E_{fd} - (X_d - X_d')\ \varDelta I_d \qquad (6.13)$$

Small deviation of Id in (6.9) are expressed as follows by coefficients using Id1, Id2, Id3 and eq. (6.11).

$$\Delta I_d = I_{d1}\,\Delta\delta t + I_{d2}\,\frac{\Delta V_t}{V_t} + I_{d3}\,\Delta\delta = I_{d1}(C_{13}\,\Delta\delta + C_{14}\,\Delta\Psi_{fd}) + I_{d2}(C_{23}\,\Delta\delta + C_{24}\,\Delta\Psi_{fd}) + I_{d3}\,\Delta\delta \qquad (6.14)$$

Substituting eq. (6.14) to eq. (6.13), relationship as follows is obtained.

$$T_{do}'\,s\,\Delta\Psi_{fd} = E_{fd} - K_3\,\Delta\Psi_{fd} - K_4\,\Delta\delta \qquad (6.15)$$

Here $K_3 = 1 + (X_d - X_d')\,(I_{d1}\,C_{14} + I_{d2}\,C_{24})$

$K_4 = (X_d - X_d')\,(I_{d1}\,C_{13} + I_{d2}\,C_{23} + I_{d3})$

Relationship as follows is directly obtained from eq. (6.11).

$$\Delta V_t = K_5\,\Delta\delta + K_6\,\Delta\Psi_{fd} \qquad (6.16)$$

Here $K_5 = V_t\,C_{23}$

$K_6 = V_t\,C_{24}$

In case of modeling induction motor load, coefficients K1 to K6 are extended as follows.

$$K_i = \frac{K_{i0} + T\,s\,K_i'}{1 + T\,s} \qquad \text{(for } i = 1 \text{ to } 6) \qquad (6.17)$$

Here, K_{i0} are stationary value regarding motor as constant power. K_i' are transient value regarding motor before speed varies as constant impedance. "s" means Laplace transform. T is a time constant that is much smaller than unit inertia constant. Here, 0.05 sec, 0.1 sec, and 0.2 sec are compared, and 0.2 sec giving worst stability is chosen.

Motion equation at the last line in eq. (6.8), eq. (6.12), (6.15), and (6.16) are synthesized, with excitation system gain GAVR, ΔP type PSS gain GPSS, speed governing system gain GGOV, block diagram as Fig. 6.4 is obtained.

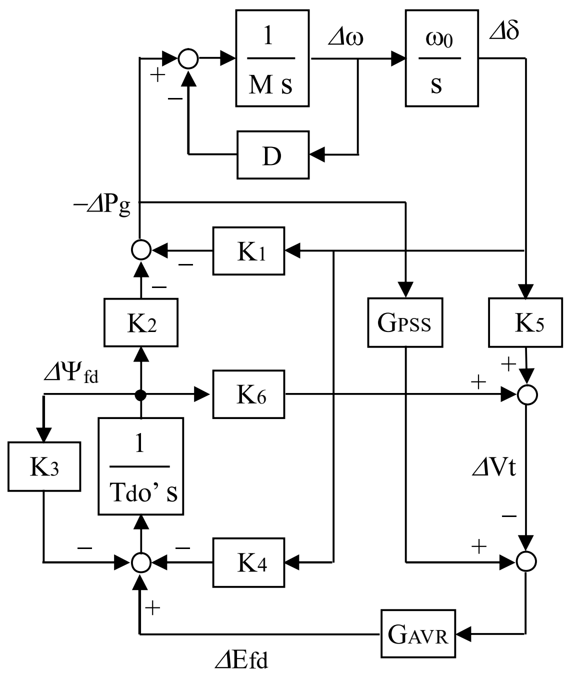

Fig. 6.4 Demello's block diagram

By block diagram in Fig. 6.4, transfer function from Δδ to ΔPg is obtained as follows.

$$\frac{\Delta P_g}{\Delta\delta} = \frac{K_1\,(K_3 + T_{do}'\,s + K_6\,G_{AVR}) - K_2\,K_4 - K_2\,K_5\,G_{AVR}}{(K_3 + T_{do}'\,s + K_6\,G_{AVR}) + K_2\,G_{AVR}\,G_{PSS}} \qquad (6.18)$$

The equation used to be expressed as follows using synchronous torque coefficient Ks and that of damping Kd .

$$\frac{\Delta P_g}{\Delta\delta} = K_s + j\,K_d \qquad (6.18')$$

However, it was difficult to distinguish whether the system is stable or unstable from information of only synchronous and damping torque coefficients. Therefore, the author plots complex values on complex plane open loop gain from $\Delta\delta$ and returns to $\Delta\delta$ as a function of swing speed, that is Nyquist's trajectory, which is used in analysis hereafter.

Damping coefficient

Damping coefficient was decide experientially. However, it can be also calculated from machine constants. On no load no excitation synchronous machine as Fig. 6.5, theory of induction motor can be applied. As to D axis, calculated as follows.

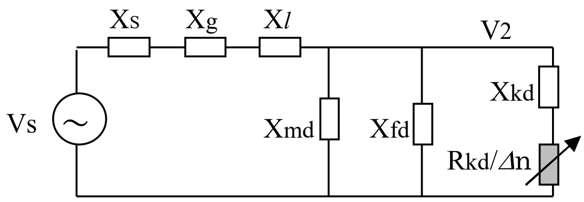

Fig. 図 6.5 Eq. D axis circuit of no load no excitation gen..

First, since Δn is very small in slight disturbance, branch Xkd is almost open. Therefore, V2 corresponding induction motor's secondary voltage is expressed as follows.

$$V_2 = \frac{X_{d'} - X_l}{X_s + X_g + X_{d'}} V_s$$

Here, Xd' is D axis transient reactance, which is expressed as follows.

$$X_{d'} = X_l + \frac{X_{md} X_{fd}}{X_{md} + X_{fd}}$$

Torque as induction motor is damping torque of synchronous generator Tk, which is equal to secondary input as induction motor, so expressed as follows. Here assumed as $X_{kd} \ll R_{kd}/\Delta n$.

$$T_k = \frac{V_2^2}{R_{kd}/\Delta n} = \left(V_s \frac{X_{d'} - X_l}{X_s + X_g + X_{d'}}\right)^2 \frac{\Delta n}{R_{kd}}$$

Therefore, damping coefficient is calculated as follows.

$$D = \frac{T_k}{\Delta n} = \left(V_s \frac{X_{d'} - X_l}{X_s + X_g + X_{d'}}\right)^2 \frac{1}{R_{kd}} \qquad (6.19)$$

As to Q axis, same calculation is possible. As a whole synchronous machine, average value of D and Q axis is used.

The calculation assumes that damping torque is derived only from damping winding, and field winding leakage reactance Xfd joins to exciting reactance Xmd, reduces secondary voltage V2, and as result reduces damping effect. The method is perhaps the most conservative one as damping assessing method. It is favorable because aim of manual calculation is screening that grasp all possible growing oscillation.

Load's voltage sensitivity

By analysis of voltage sag records, it found to be adequate to model load as mix of 50% induction motor and 50%constant impedance[11]. Capacitor that compensates no load reactive power is added to motor terminal. Parameters derived from voltage sag analysis and experiment at motor capacity (kVA) base: active power Pm (kW) is 0.5, restraint reactance Xm is 0.2, therefore motor reactive power Qm (kVar) is $0.2*0.5^2 = 0.05$, and as result, Qm/Pm ratio is 0.1. Also constant impedance's Qz/Pz ratio is assumed as 0.1.

Motor's active power has constant power character. Therefore, motor current is inverse proportional to voltage. Since motor's reactive power is loss by restraint reactance, it is inverse proportional to squared voltage. As negative voltage sensitivity is unbelievable, evidence is shown. Fig. 6.6 is voltage dependent power of existing pump-motor. Loaded reactive power when no load reactive power is just compensated by capacitor certainly shows negative voltage sensitivity.

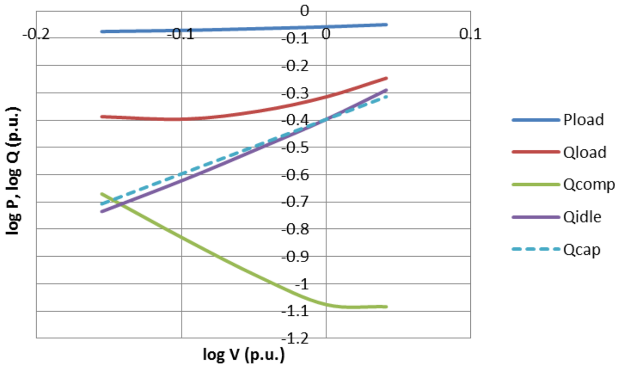

Fig. 6.6 Voltage dependent Power of existing motor

Load's voltage sensitivity changes if seen via reactance. In Fig. 6.7 active and reactive power is P+ jQ at receiving end and is Ps + jQs at sending end. Load's voltage sensitivity of active and reactive power are α, β at receiving end and are αs, βs at sending end. Voltage at sending and receiving end are calculated as follows.

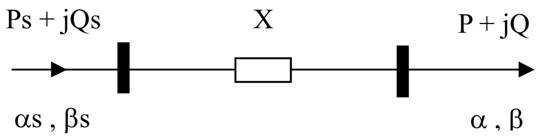

Fig. 6.7 Load's voltage sensitivity seen via reactance

$$Vs^2 = V^2 + 2XQ + \frac{X^2}{V^2}(P^2 + Q^2)$$

Take small deviations of that.

$$Vs^2\frac{\Delta Vs}{Vs} = \{V^2 + XQ\beta + \frac{X^2P^2}{V^2}(\alpha - 1) + \frac{X^2Q^2}{V^2}(\beta - 1)\}\frac{\Delta V}{V}$$

So, voltage change amplifying factor κ is calculated as follows.

$$\kappa = \frac{\Delta Vs/Vs}{\Delta V/V} = \frac{V^2 + XQ\beta}{Vs^2} + \frac{X^2\{P^2(\alpha - 1) + Q^2(\beta - 1)\}}{Vs^2V^2} \qquad (6.20)$$

Using it, active power 's voltage sensitivity at sending end αs is calculated as follows.

$$\alpha s = \frac{\Delta Ps/Ps}{\Delta Vs/Vs} = \frac{\Delta P/P}{\Delta V/V}\ \frac{\Delta V/V}{\Delta Vs/Vs} = \frac{\alpha}{\kappa} \qquad (6.21)$$

Reactive power at sending end is expressed as follows.

$$Qs = Q + \frac{X(P^2 + Q^2)}{V^2}$$

Take small deviation of that.

$$Qs\beta s\frac{\Delta V_s}{V_s} = \{\Theta\beta + \frac{2XP^2}{V^2}(\alpha - 1) + \frac{2XQ^2}{V^2}(\beta - 1)\}\frac{\Delta V}{V}$$

So, voltage sensitivity of reactive power at sending end βs is calculated as follows.

$$\beta_s = \frac{Q\,\beta}{Qs\,\kappa} + \frac{2XP^2(\alpha - 1) + 2XQ^2(\beta - 1)}{Qs\,\kappa\,V^2} \tag{6.22}$$

Load's frequency sensitivity

Frequency sensitivity of active power has damping effect on power swing. There is a relationship shown in Fig. 6.8 between generator slip $\Delta\omega$ and load's frequency change Δf.

Load's active power change during swing ΔP_L is expressed as follows.

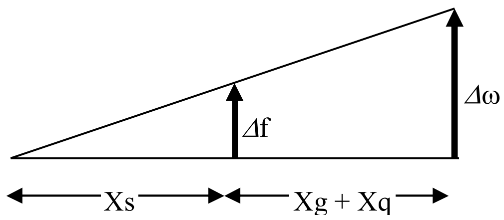

Fig. 6.8 Generator slip and load's frequency change

$$\Delta P_L = \alpha_{FL}\,P_L\,\Delta f = D_L\,Wg\,\Delta\omega$$

P_L is active power, α_{FL} is frequency sensitivity, Δf is frequency deviation of load, Wg is capacity, $\Delta\omega$ is slip of generator. D_L is additional damping by load. Thus, D_L is expressed as follows.

$$D_L = \frac{\alpha_{FL}\,P_L\,Xs}{Wg\,(Xs + Xg + Xq)} \tag{6.23}$$

Here for conservative, only motor input power being proportional to squared speed is considered.

Modeling of RE

As major RE is PV (Photovoltaic generation) in Japan, Also PV's character is supposed here. Power swing has around 2 sec period, which PV's MPPT cannot follow, and ACR control is dominant in PV. Therefore, PV is modeled as negative constant current load.

Impact of anti-islanding

As impact of anti-islanding that is obligated to equip in RE, reduction of damping coefficient and reduction of PSS effect are listed up.

Reduction of damping coefficient is, though it is rough assessment, can be calculated as follows. Here, fr is load bus frequency.

$$D_{ISL} = \frac{\Delta fr}{\Delta\omega}\,\frac{\Delta Q_{RE}}{\Delta fr}\,\frac{\Delta V_r}{\Delta Q_{RE}}\,\frac{\Delta P_r}{\Delta V_r}\,\frac{1}{Wg} \tag{6.24}$$

The equation express degree of the impact: generator accelerates=>RE frequency rizes=>RE absorbs reactive power=>load voltage drops=>load power decreases=.generator accelerates. Factors are calculated as follows.

$$\frac{\Delta fr}{\Delta\omega} = \frac{Xs}{Xs + Xg + Xq}$$

$$\frac{\Delta Q_{RE}}{\Delta fr} = W_{RE}\,\frac{G_{ISL}}{1 + T_{ISL}\,s}\,\frac{T_r\,s}{1 + T_r\,s}$$

G_{ISL} is gain of anti-islanding. Here assumed 50% reactive power of RE rated capacity W_{RE} is generated by 1 Hz frequency change. Therefore, gain is -30 p.u.. T_{ISL} is time constant of low pass filter, here 0.05 sec. Tr is time constant of high pass filter, here 0.2 sec.

$$\frac{\Delta Vr}{\Delta Q_{RE}} = X_{RESYS}$$

X_{RESYS} is reactance seen from RE to system side.

Active power's voltage index on mixed 50% motor and 50% impedance is 2 at transient and 1 at stationary. That of RE is 1at both transient and stationary. Therefore, total indices of load and RE (α at stationary, αr' at transient) are obtained, are linked by the time constant T (already introduced) smoothly, and is expressed as follows.

$$\frac{\Delta Pr}{\Delta Vr} = \frac{\alpha_r + T\,s\,\alpha_r'}{1 + T\,s}\;\frac{Pr}{Vr}$$

Next, reduction of PSS effect is, though rough, van be assessed as follows.

$$G_{PSS\,ISL} = \frac{\Delta fr}{\Delta\omega}\;\frac{\Delta Q_{RE}}{\Delta fr}\;\frac{\Delta Vt}{\Delta Q_{RE}}\;\frac{1}{Wg\,(M\,s + D)} \qquad (6.25)$$

Two of factors in right side is already calculated in damping reduction. the others one is calculated as follows.

$$\frac{\Delta Vt}{\Delta Q_{RE}} \qquad \frac{Xs\,Xd'/Wg}{Xs + Xg + Xd'/Wg}$$

This is ratio of generator voltage rise ΔVt by RE reactive power increase ΔQ_{RE}.

By calculations above, gain from speed up $\Delta\omega$ to generator voltage rise ΔVt is obtained. That is operation of $\Delta\omega$ type PSS itself. To translate equivalently to usual ΔP type PSS gain, 1/Wg (M s + D) os multiplied. The reason being divided by generator capacity Wg is that generator with educed capacity tends to receive impacts.

Example of sending system[8]

Structure of example power sending system is shown in Fig. 6.9. A one circuit trip (without grounding) on double circuit line is modeled at F1. Power flow condition after trip is shown in Table 6.1.

Table 6.1 Power flow condition od sending system after fault

Xt	Xs	Vt	Vb	Vs	Pg	Pb	Ps
0.2061	4.7804	1.025	1.0	1.0	0.7601	0.6971	0.0629

Existing load is mix of motor and impedance. Total voltage sensitivity varies by motor ratio. Further affected by structure of Fig. 6.2, sensitivity seen from system is different from that of load itself. Calculated result on the example sending system is introduced. Parameters of the example sending system is shown in Table 6.2.

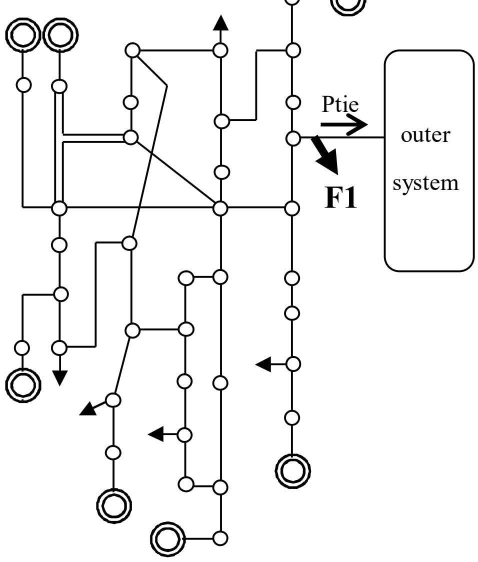

Fig. 6.9 Structure of sending system

Calculated load's voltage sensitivity at load bus, medium bus, and trunk bus are shown in Fig. 6.10. It must be noticed that voltage sensitivity reactive load at trunk bus takes a large negative value. Much amount of capacitor equipped at medium bus largely influences that.

Table 6.2 Load in sending system (load terminal base)

Xm	Xr	Xi	Vb	Vm	Vr
0.246459	0.184815	0.1	1.0	1.0	0.960171

Pb + jQb	Pm + jQm	jQmc	Pr + jQr
1.0+j0.12560	1.0+j0.312656	j0.437816	1.0+j0.109775

Demello's coefficients When motor ratio is changed, stationary Demello's coefficients vary as Fig. 6.11. Demello's coefficients indicate stable side if positive and unstable side if negative. As influence by the other factors, it is impossible to judge stable or unstable by Demello's coefficient, but they can be use as reference.

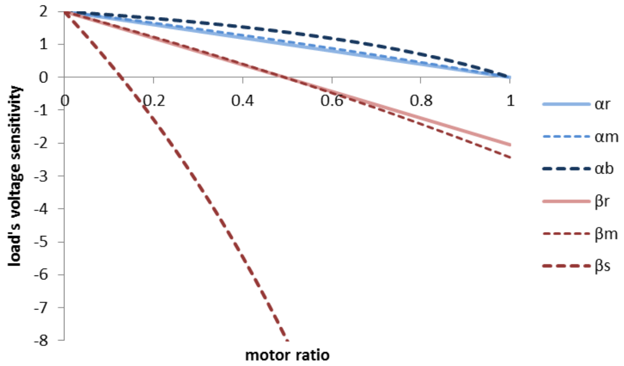

Fig. 6.10 Load' voltage sensitivity by location (Sen.)

At a glance, a singular point appears at motor ratio is around 70%. In larger motor ratio K2 turns to negative. This means when rotor magnetic flux is enforced generator output decreases. Under such condition, stabilization is impossible by any excitation systems.

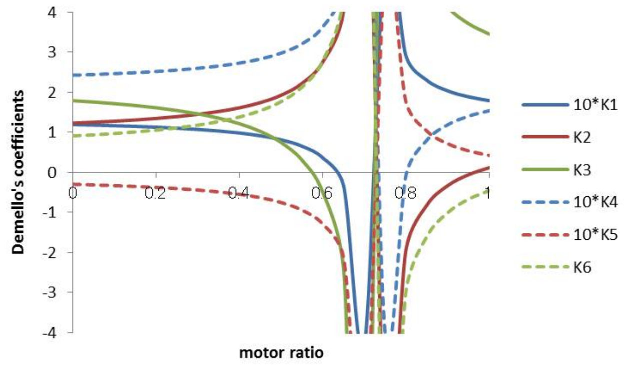

Fig. 6.11 Demello's coefficients by motor ratio (Sen.)

Even when motor ratio is zero, K5 takes negative value. That is typical character of power sending system. Since generator itself has some damping, such a light negative K5 cannot result oscillatory instability. However, major reason that power swing appear more frequently in sending system lies here.

As motor ratio increases, negative K5 value increases, and oscillatory instability appears before reaching to the singular point. Following it, K3 and K1 turn to negative. That is, motor load's influences to reduce oscillatory stability. Oscillatory stability limit is strongly affected by negative K5, but instability caused by negative K3 and K5 can be improved by excitation system design.

Impact by load model Difference in stationary Demello's coefficient by load model is shown in Table 6.3.

Table 6.3 Stationary Demello's coefficients by load model (Sen.)

Agg.	Load	αb	βbQb	K_1	K_2	K_3	K_4	K_5	K_6
3E	IM	1.3527	-0.9678	0.0855	1.8442	0.7529	0.2970	-0.0725	1.7134
2E	IM	1.0534	-0.3645	0.1360	0.9270	0.9232	0.2871	-0.0384	1.0851
3E	CI	1.2248	-0.6979	0.1116	1.3613	0.8189	0.2934	-0.0555	1.3924
3E	CI	1.0217	-0.1494	0.1415	0.8238	0.9959	0.2833	-0.0336	0.9923
*	CZ	2	0.2503	0.1190	1.2266	1.7877	0.2424	-0.0299	0.9085

Load is modeled as motor 50% (IM), constant current (CI, but reactive power is CZ), and constant impedance (CZ). Aggregation is done by three-element method (3E) and two-element method. 3*2=6 cases are possible, but results of 3E and 2E become equal, 5 cases are considered. Transient Demello's coefficients are equal tu those of CZ case. Slow excitation system with PSS are modeled. Load's voltage sensitivity seen from trunk bus is written. That of reactive power is expressed by product of βb and Qb. K5 takes the largest negative value in IM load and 3E aggregation case. These five load model are compared. Damping torque coefficients are shown in Fig, 6.12. In IM load and 3E aggregation case large negative damping torque appears. IM load and 2E aggregation follows. In CI or CZ load cases, large negative values do not appear.

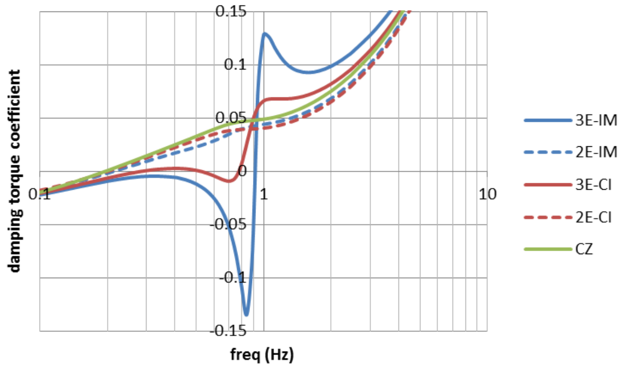

Fig. 6.12 Damping toque coefficients by load model (Sen.)

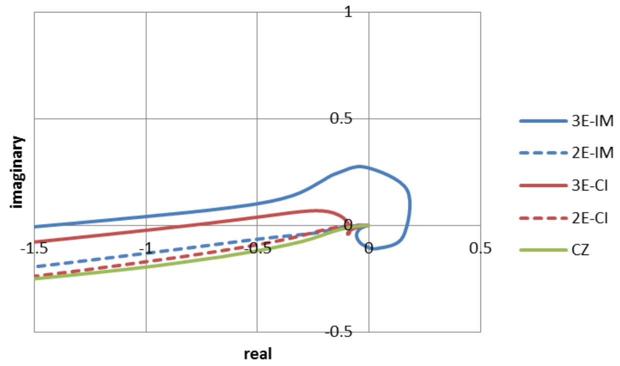

Fig. 6.13 Nyquist's trajectories by load model (Sen.)

As concrete stability distinction is impossible by damping torque coefficient, Nyquist's trajectory is employed for the purpose. That is open loop gain plotted on complex plane as increasing frequency. The results are shown in Fig. 6.13. As frequency increases, trajectory converges to zero. In the process, if point (-1, 0) is seen always in left side, the system is stable. In the figure, IM load and 3E aggregation case is slightly unstable, IM load and 2E aggregation is slightly stable, the other three cases are quite stable.

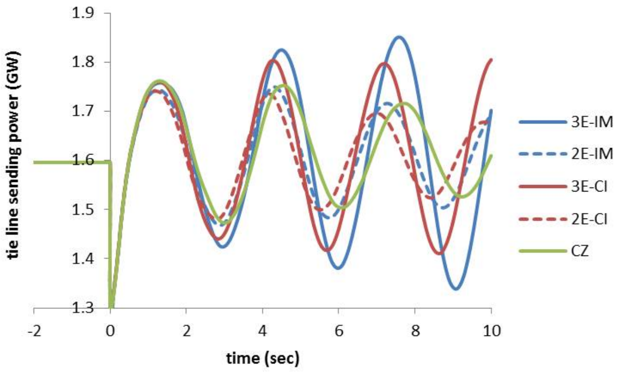

Fig. 6.14 Swing simulation results by load model (Sen.)

Simulation result on detailed model are shown in Fig. 6.14. IM load and 3E aggregation shows growing swing, IM load and 2E aggregation shows continuous swing. The other cases show decaying swing. Simulation results well agree with Nyquis's trajectory analyses.

Impact of excitation system design Oscillatory stability is much affected by excitation system design. To clarify the impact, common system as Fig. 6.15 is applied to all generators. Two parameters exist.

Exciter time constant Te: 2 sec (slow), 0.5 sec (fast)

PSS gain Gp: 0.5 (use), 0.0 (lock)

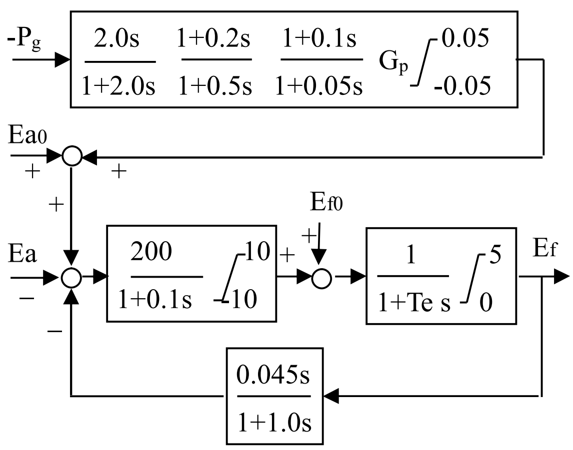

Fig. 6.15 Supposed excitation system

Four design on excitation system are examined. Difference of slow and fast excitation systems are shown in Bode diagram in Fig. 6.16. At typical power swing frequency (0.5Hz) gains do not large difference, but angle is slow system is by 30 deg. lagging. Angle lagging spoils stability in any feedback system. So, oscillatory stability becomes poor in slow excitation system.

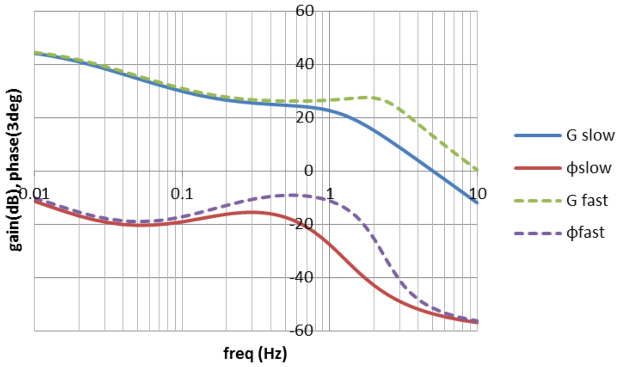

図 6.16　Bode diagram of slow and fast excitation systems

Oscillatory stability by the four excitation system design is examined. Most realistic 50%IM load and 3E aggregation is adopted. Damping torque coefficient is shown in Fig. 6.17. The coefficient is negative at 1 Hz swing or slower without PSS, is still negative if PSS is used in slow excitation system, and turns positive only fast excitation with PSS case.

As concrete stability distinction is impossible by damping torque coefficient, Nyquist's trajectory is employed for the purpose. That is open loop gain plotted on complex plane as increasing frequency. The results are shown in Fig. 6.18. As frequency increases, trajectory converges to zero. In the process, if point (-1, 0) is seen always in left side, the system is stable. In the figure only fast excitation system with PSS case i stable.

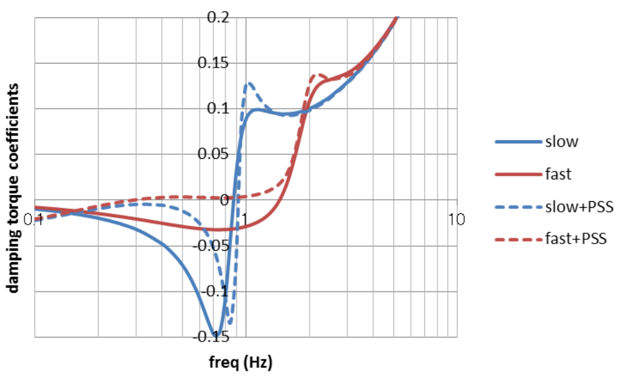

Fig. 6.17　Damping torque by excitation system design (Sen.)

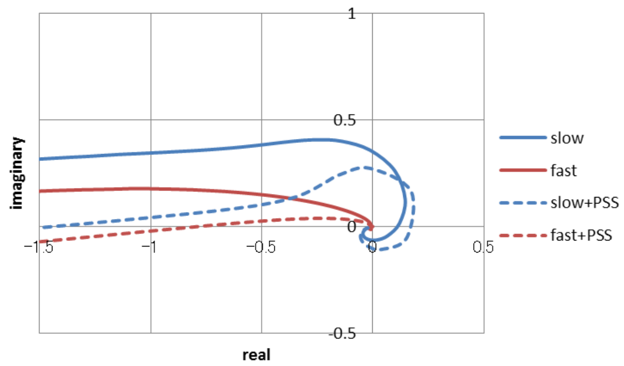

Fig. 6.18　Nyquist's trajectory by excitation system design (Sen.)

At last verified by simulation. The result is shown in Fig. 6.19. Only fast excitation system with PSS case shows decaying swing, and the other show continuous or growing swing. Simulation result well agrees with Nyquist's trajectory analysis. Thus in power sending system, first adopting PSS, ans second making excitation system response fast are special cures for oscillatory stability improvement.

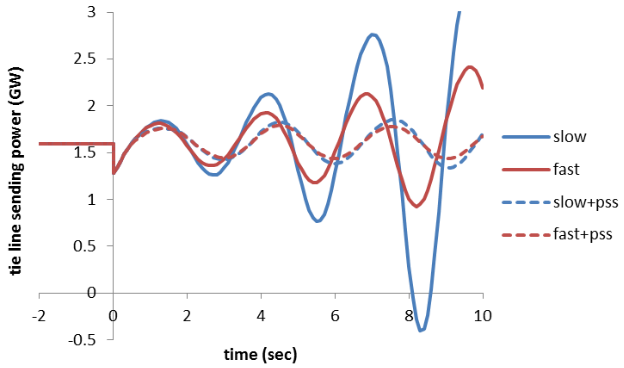

Fig. 6.19　Power swing by excitation system design (Sen.)

Impact of RE design　RE supply 20% of load, some conventional generators stop due to balance. As RE design, FRT type and DVS type. In oscillatory stability deep voltage sag is not assumed, so drop type shows the same result of FRT type. Slow excitation system with PSS is assumed. Most realistic IM50%load and 3E aggregation load model is adopted.

Damping torque coefficient is shown in Fig. 6.20. Comparing no RE case, FRT type shows better stability, and DVS type shows much better stability.

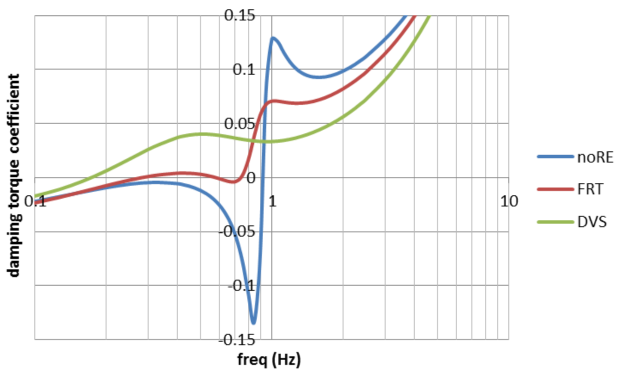

Fg. 6.20 Damping torque RE coefficient by RE design (Sen.)

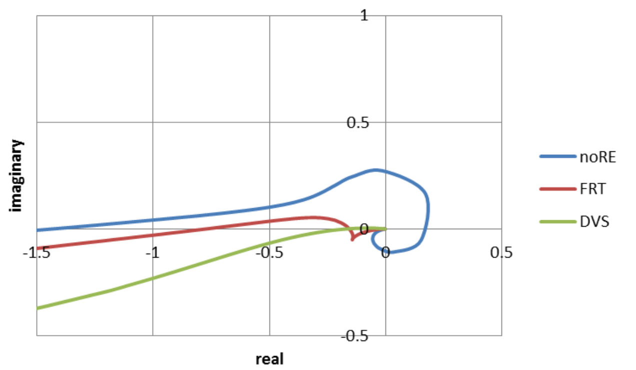

Fig. 6.21 Nyquist's trajectory by RE design (Sen.)

Nyquist's trajectory is shown in Fig. 6.21. No RE case is slightly unstable, FRT type case is slightly stable, and DVS type case is quite stable.

Simulation result in detailed system is shown in Fig. 6.22. Compared with no RE case, FRT type case is better but still unstable different from Nyquist' trajectory. The reason is thought that aggregation when making model for Nyquist's trajectory has brought some error. DVS type case is quite stable.

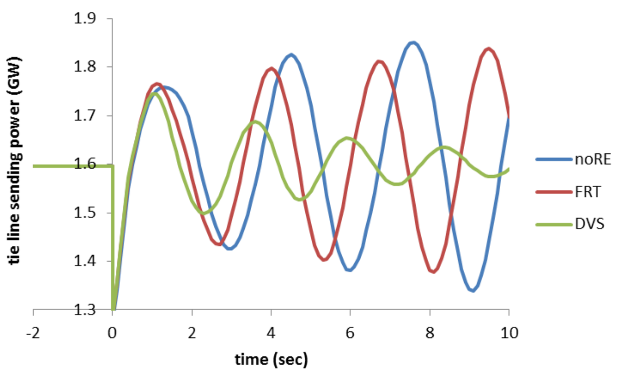

Fig. 6.22 Power swing aspect by RE design (Sen.)

As stated above, on oscillatory stability of power sending system, it is found that FRT type RE has a little stabilizing effect, and DVS type FRT has very strong stabilizing effect.

Example power receiving system(8)

Structure of the power receiving system is shown in Fig. 6.23. The system receives much power from outer system via three tie line. Assume one tie line is lost by fault without grounding at F1. As the result the system turns to a narrow and long system receiving much power via tie line 1 and 2. Power flow condition after fault is shown in Table 6.4.

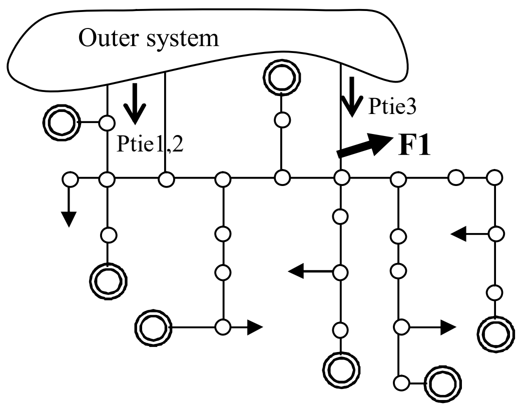

Fig. 6.23 Structure of the receiving system

Table 6.4 Power flow condition of the receiving system

Xt	Xs	Vt	Vb	Vs	Pg	Pb	Ps
0.1259	1.5990	1.02	1.0	1.0	0.8175	1.1021	-0.2846

Also load characteristics is calculated in receiving system. Parameters are shown in Table 6.7. Calculation results are shown in Fig. 6.23. The result are shown in Table 6.24. Similarly as sending system sensitivity of load's reactive power seen from trunk bus takes a large negative value.

It is natural that both sending and receiving systems show similar load character seen from trunk bus. Because difference between the two systems is only difference of generator output, and structure of load under trunk bus is similar. That is understood by the fact that parameters are not much different between sending both systems.

Table 6.5 Load's parameter of receiving system (load power base)

Xm	Xr	Xi	Vb	Vm	Vr
0.290402	0.155867	0.1	1.0	1.0	0.952890
Pb + jQb	Pm + jQm	jQmc	Pr + jQr		
1.0+j0.184401	1.0+j0.281792	j0.397668	1.0+j0.110132		

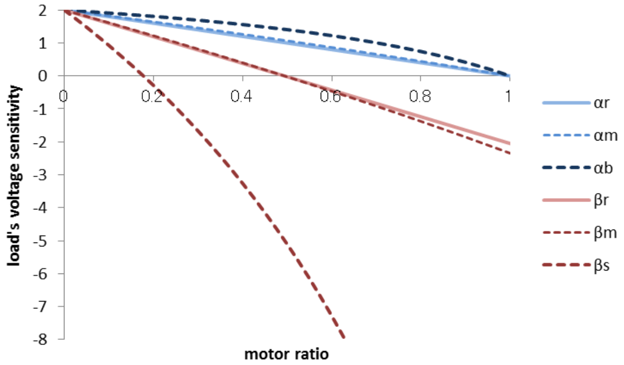

Fig.6.24 Load's voltage sensitivity by location (Rec.)

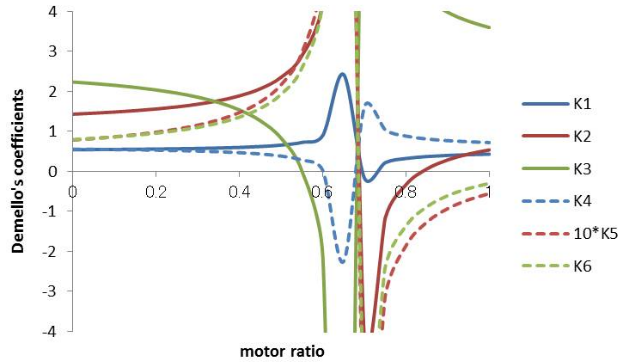

Fig. 6.25 Demello's coefficients by motor ratio (Rec.)

Demello's coefficients When motor ratio id changed, stationary Demello's coefficients vary as Fig. 6.25. At a glance a singular point exists around 70% motor ratio. At higher motor ratio, K_2 turns negative. This means when rotor magnetic flux is enforced, generator output decreases. In such a condition, no excitation system can cure instability.

At zero motor ratio all Demello's coefficients are positive. This is a typical receiving system's character, and possibility of oscillatory instability is very low. However, as motor ratio increases, K_3 turns to negative at first. Next K_4 turns to negative. Therefore, motor load acts to spoil oscillatory stability of negative K_3 type. The type is different phenomenon from usual oscillatory instability (power swing) by negative K_5. Instability caused by negative K_3 and K_4 can be improved by excitation design.

Impact of load model On the same five load model as sending system, load's voltage sensitivity and stationary Demello's coefficients are shown in Table 6.6.

Table 6.6 Load's voltage sensitivity and Demello's coefficients (Rec.)

縮約	負荷	αb	βbQb	K_1	K_2	K_3	K_4	K_5	K_6
Y	IM	1.4051	-0.9421	0.6561	2.3532	0.8239	0.3809	0.2168	1.9266
T	IM	1.0718	-0.2893	0.5602	1.0935	1.2792	0.5329	0.0979	0.9975
Y	CI	1.2488	-0.6288	0.5642	1.6159	0.9709	0.3990	0.1564	1.4330
T	CI	1.0319	-0.0768	0.5485	0.9938	1.3756	0.5440	0.0866	0.8986
*	CZ	2	0.2967	0.5495	1.4984	2.2261	0.5744	0.0834	0.8229

Damping torque coefficient is shown in Fig. 6.26. Three cases by two-element aggregation or constant impedance are stable. Three-element aggregation reflecting reality brings unstable tendency. In the most faithful three-element aggregation and IM50% load case, significant instability appears.

Nyquist's trajectory is shown in Fig. 6.27. Similar to damping, three-element aggregation cases show poor oscillatory stability, and go unstable with IM50% load.

Simulation result on detailed system is shown in Fig. 6.28. Slow excitation system with PSS is assumed. Three-element aggregation cases show poor stability, and go unstable with IM50% load.

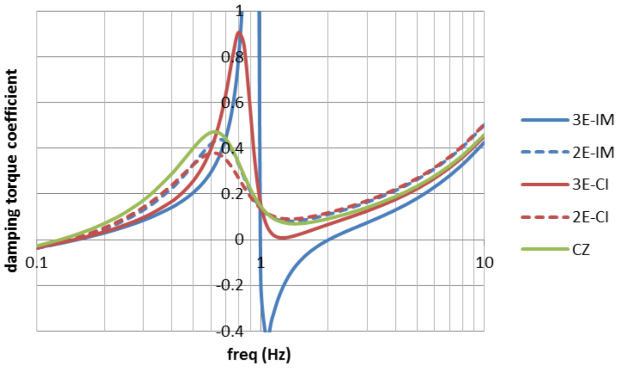

Fig. 6.26 Damping torque coefficient by load model (Rec.)

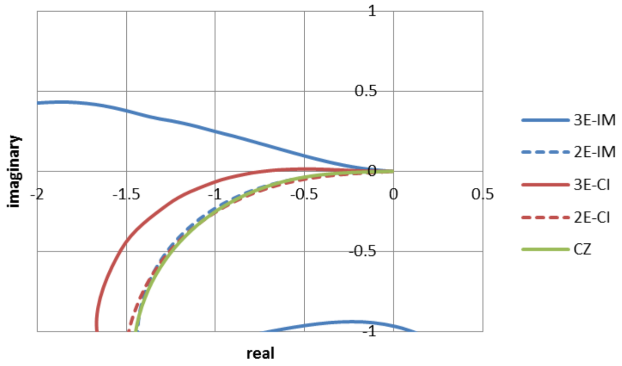

Fig. 6.27 Nyquist's trajectory by load model (Rec.)

Simulation result well agree with Nyquist's trajectory analysis.

As stated above, Comparing to three-element aggregation and IM50% load case that faithfully reflects reality, the other load model give optimistic assessment. It must be pointed out that present load model that never reflect reality brings risk to overlook possible oscillatory instability.

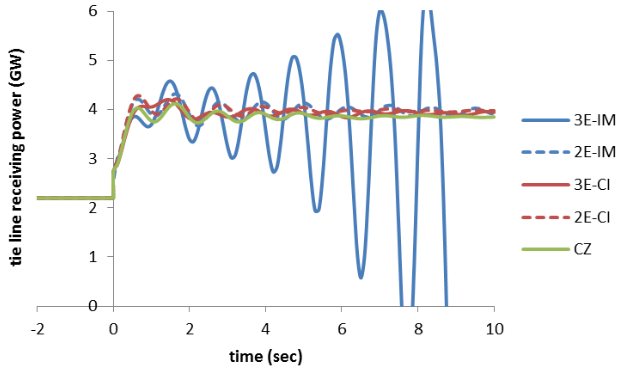

Fig. 6.28 Power swing aspect by load model (Rec.)

Impact of excitation system design Similar four excitation system as sending system are compared. Load model is realistic three-element aggregation and IM50% load. Damping torque coefficient is shown in Fig. 6.29. In slow excitation system cases damping goes negative at 1 Hz or faster. Even with PSS, negative damping range shifts to higher frequency but remain. So long as using slow excitation system, instability is never solved.

Nyquist's trajectory is shown in Fig. 6.30. Stability is poor in slow excitation system cases, and PSS that is believed as special cure shows negative effect. Fast excitation cases show good stability without concerning PSS.

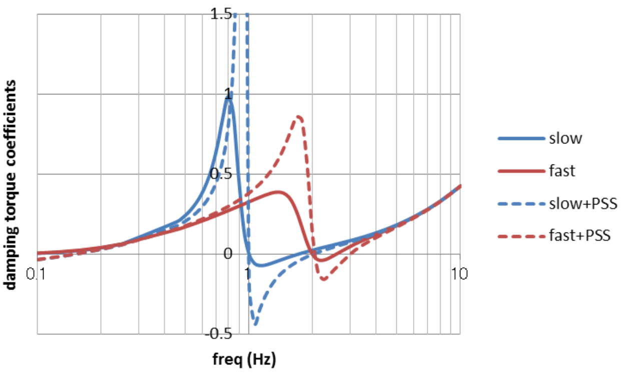

Fig. 6.29 Damping torque by excitation system design (Rec.)

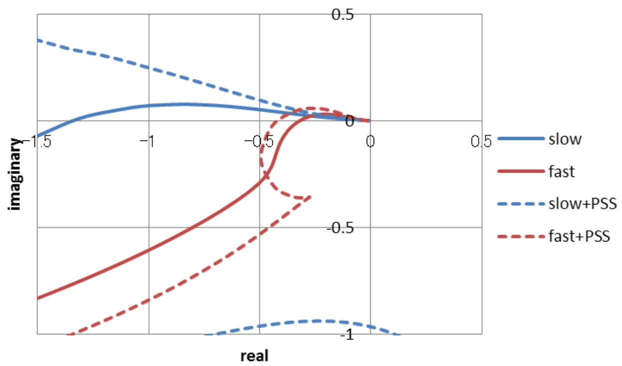

Fig. 6.30 Nyquist's trajectory by excitation system design (Rec.)

Simulation result in detailed system is shown in Fig. 6.31. Fast swing having 1 Hz period grows in slow excitation system cases, PSS certainly shows negative effect. By fast excitation system swing is stabilized, but without PSS case shows unstable result than Nyquist's trajectory analysis. The reason is thought that aggregation error exists in Nyquist's trajectory analysis. Different from sending system, in receiving system, first high speed excitation system, second adopting PSS are ultimate measure for oscillatory stability improvement.

Impact of RE design Similar to sending system RE supply 20% of load and partial conventional power source stop due to balance. RE design is assumed FRT type and DVS type. In oscillatory stability deep voltage sag is not assumed, therefore, drop RE gives the same result of FRT type RE. Slow excitation system with PSS is assumed. Realistic three-element aggregation and IM50% load is assumed.

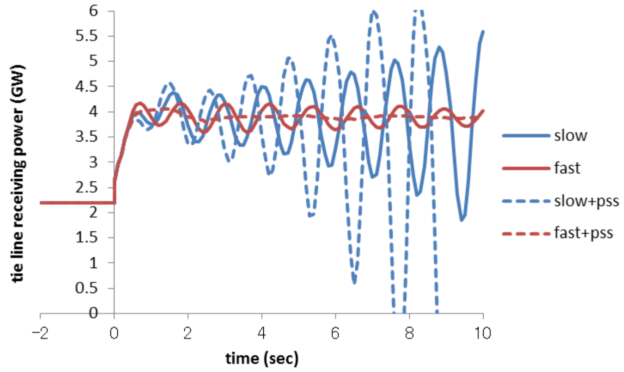

Fig. 6.31 Power swing and excitation system design (Rec.)

Damping torque coefficient is shown in Fig. 6.32. FRT type case is not stable than no RE case. DVS type case is quite stable. Nyquist's trajectory is shown in Fig. 6.33. FRT type case is not stable than no RE case. DVS type case is quite stable.

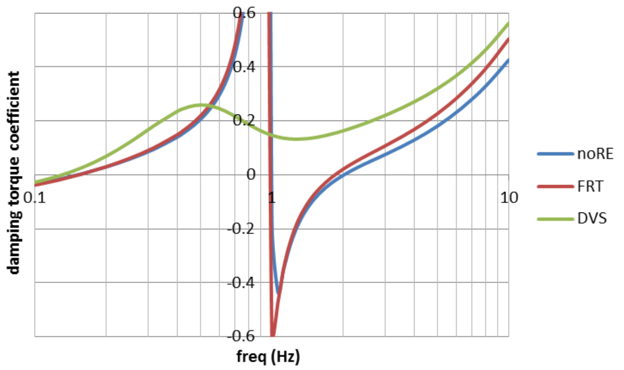

Fig.. 6.32 Damping torque coefficient by RE design (Rec.)

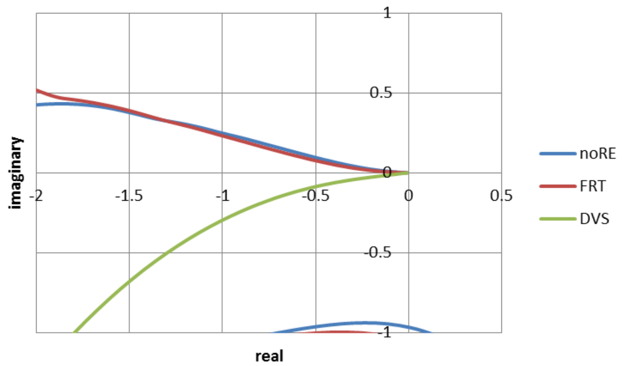

Fig. 6.33 Nyquist's trajectory by RE design (Rec.)

Simulation result in detailed system is shown in Fig. 6.34. FRT type case becomes rather worse than no RE case, and is worse than Nyquits's trajectory analysis. The reason is thought that aggregation to build model for Nuquist's trajectory brought some error. DVS type case shows quite well stability.

As stated above, FRT type does not have stabilizing effect on oscillatory stability in receiving system at all, but on the contrary, DVS type RE has strong stabilizing effect.

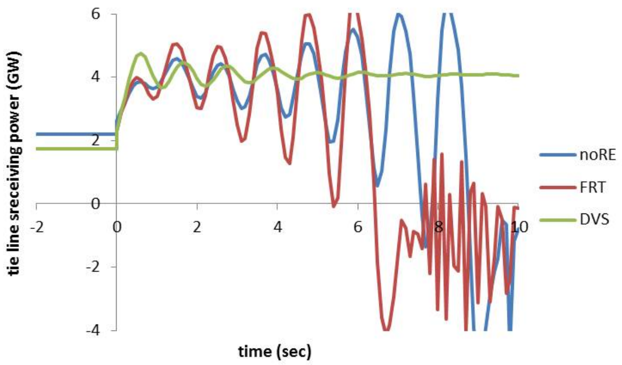

Fig. 6.34 Power swing aspect by RE design (Rec.)

Deep-rooted misunderstanding

Instability of power receiving system was first introduced in Central Electric Power Council "Investigation Working Group on Impact to Trunk System by Distributed Generation". Considering motor load and load brabch, IEEJ EAST30 and WEST30 power system models are remodeled. Then, whole system became unstable, power swing is seen not only in sending system but also in receiving system. WG member said that the author's model with motor load and load branch is false because such power swing does not exist in receiving system. Howevwe, IEEJ EAST30 and WEST30 model adopt slower excitation system than “”slow system” in the chapter. Thus, remarkable power swing occurred in receiving system. Existing excitation system is much faster, so power swing never appar in existing receiving system. According to these misunderstanding, impact of excitation system design in both sending and receiving system is minutely studied.

Oscillatory stability is the most difficult phenomenon for analysis based on mathematics and physics. Therefore, engineers who analyze by methods except simulation are quite rare, and already retired today. Because of difficulty any inheritors do not exist. To not be solved except by simulation means that mechanism of instability is unknown, therefore, countermeasure is not reasonably found. The author thinks that these situation must be improved, but “wall against fool” still stand severely as Dr. Yoro says.

Growing swing of islanded system

Growing swing phenomenon that small generator angle swing grows by time is usually occurs between two groups in loosely interconnected large system, hardly occur in tightly interconnected islanded system. However, another kind of growing swing can occur. Here, its mechanism is cleared theoretically. Also major factors affecting the phenomenon. Theory is verified by simulation. At last, preparing f or high RE integration, one suggestion is presented.

Model system and flow condition　Here, an existing power system interconnecting to 500kV/275kV substation via one double-circuit transmission line is taken as example. It is aggregated into one machine one load infinite bus system model. Since aggregated islanded system has only one generator, angle swing cannot occur.

Y-connection method(12) is used in aggregation. Assuming short circuit current from 500kV side as 40kA in the 500kV/275kV substation, infinite side impedance is calculated. Structure of the model system is shown in Fig. 6.35 with power flow at 25% synchronous generator (SG) ratio. Branch impedance expressed by π form equivalent circuit is shown in Table 6.7.

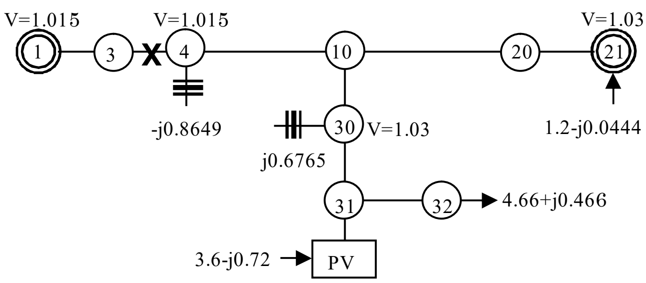

Fig. 6.35　Structure of model system (aggregated)

Table 6.7　Impedance of model system (at 1GVA base)

br	from	to	R	X	Y/2
3	1	3		0.02887	
4	3	4		0.04533	
10	4	10	0.00322	0.07234	0.51141
20	10	20	0.00080	0.00817	0.19451
21	20	21		0.09640	
30	10	30	-0.00024	0.01707	0.13046
31	30	31	0.00036	0.01748	0.07933
32	31	32	0.00614	0.01228	

Node 1 is infinite bus. Node 3 is 500kV bus of the 500kV/275kV substation. Node 4 is its 275kV bus of the substation, where much reactive power source (capacitor, reactor) locates. The example includes cable transmission lines in urban area, and much reactor is operating. Branch 21 is main transformer of aggregated generator, and ita impedance inversely proportional to generator capacity. Node 30 is 66kV class bus, where much capacitor is equipped. Node 31 is 6kV bus, where PV interconnects. Node 32 is low voltage bus, where load exists. By opening at right side of branch 3 to 4, islanded system appears.

Theoretical analysis method　Oscillatory stability analysis in islanded system can regard a special case of oscillatory stability analyzed by Komami-Komukai theory introduced in the beginning of the chapter.

In one machine one load infinite bus system, by calculating small deviations around equilibrium in system side than generator terminal, relationship as eq. (6.7) was obtained. Variables in system side than generator terminal are not used in analysis hereafter.

$$\begin{pmatrix} \Delta Pg \\ \Delta Qt \end{pmatrix} = \begin{pmatrix} Pg_1 & Pg_2 \\ Qt_1 & Qt_2 \end{pmatrix} \begin{pmatrix} \Delta\delta t \\ \dfrac{\Delta Vt}{Vt} \end{pmatrix} \qquad \text{(6.7) again}$$

Here, expressing voltage sensitivities of active and reactive power at generator terminal after islanded as α and β, the four elements in the matrix above is calculated as follows.

$$\left.\begin{aligned} Pg_1 &= 0 \\ Pg_2 &= \alpha\, Pg \\ Qt_1 &= 0 \\ Qt_2 &= \beta\, Qt \end{aligned}\right\} \qquad (6.26)$$

By conditions $Pg_1 = 0$ and $Qt_1 = 0$, relationships as follows exist in eq. (6.10).

$$Id_3 = -Id_1\,, \qquad Iq_3 = -Iq_1$$

As the result, equations as follows are conducted.

$$B_{11} = B_{13}\,, \qquad B_{21} = B_{23}$$

Then, in eq. (6.11),

$$C_{13} = 1\,, \qquad C_{23} = 0$$

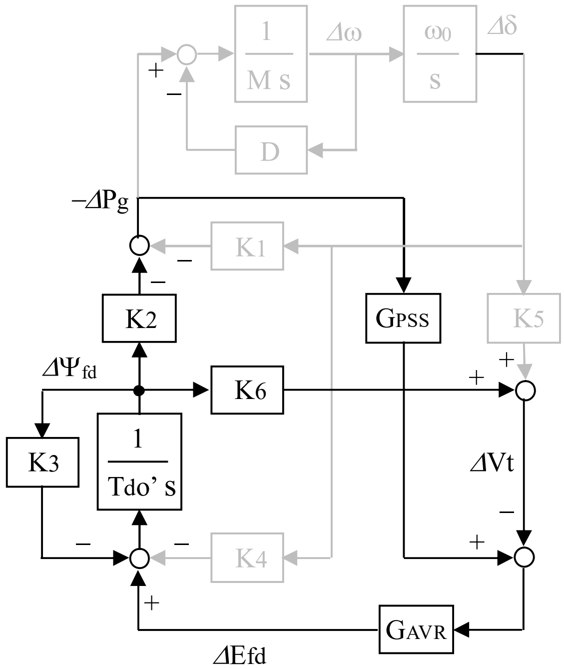

Fig. 6.36 Demello's block diagram in islanded sys.

Thus, three out of the six Demello's coefficients become zero as follows.

$$K_1 = Pg_1\, C_{13} + Pg_2\, C_{23} = 0$$

$$K_4 = (Xd - Xd')\,(Id_1\, C_{13} + Id_2\, C_{23} + Id_3 = 0$$

$$K_5 = Vt\, C_{23} = 0$$

Block diagram shown in Fig. 6.4 becomes to Fig. 6.36, where gray parts is not needed. The system can be recognized as a feedback system with ΔEfd as input and $\Delta\Psi fd$ as output. Its open loop gain is expressed as follows.

$$G(s) = \frac{1}{Tdo'\,s}\,\{K_3 + K_6\, G_{AVR} + K_2\, G_{PSS}\, G_{AVR}\} \qquad (6.27)$$

de Mello's coefficients Stability of the feedback system shown in Fig. 6.36 is spoiled when de Mello's coefficients K_2, K_3, and K_6 go negative. When proportion of synchronous generator output among all power sources (SG ratio) changes, PV output changes. Generally, voltage sensitivity is different between load and RE. Therefore, appeared voltage sensitivity of residual load seen from generator terminal will change by SG ratio.

Taking α = 1 and β = 2, which are generally used in static load model, as standard, and varying appearing voltage sensitivity seen from generator terminal : α and β, de Mello's coefficients vary as shown in Fig. 6.37. Negative α gives negative K2 and K3. K6 never go negative. When voltage sensitivity of load's active power α_L is low, and that of PV α_{PV} is high, α tends to go negative.

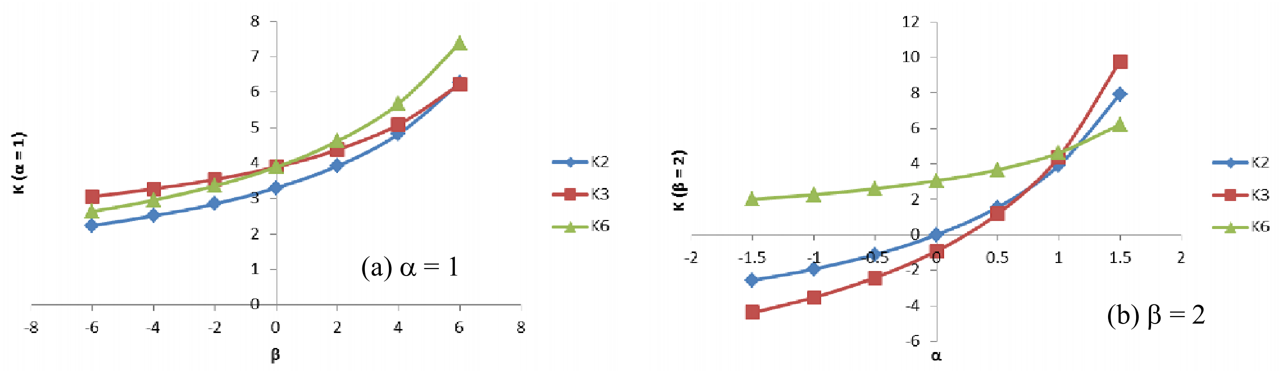

Fig. 6.37 de Mello's coefficients by load's voltage sensitivity in islanded system

Nyquist's trajectory Generator constants are shown in Table 6.8. Excitation system is shown in Fig. 6.38.

Table 6.8 Generator constants

Xd	Xd'	Xq	Tdo'
1.8	0.3	1.75	6.0sec

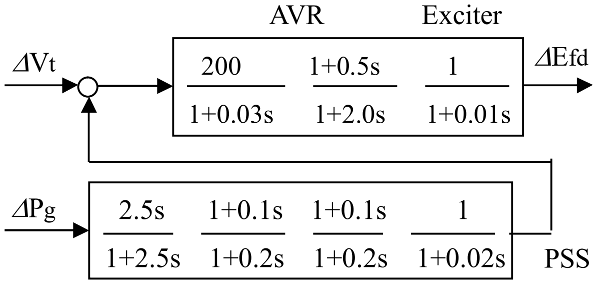

Fig. 6.38 Design of excitation system

With Fixed β = 2, Nyquist's trajectories by varying α are shown in Fig. 6.39. When α = -1.0 and -1.2, the system is stable. When -1.3 and -1.5, unstable.

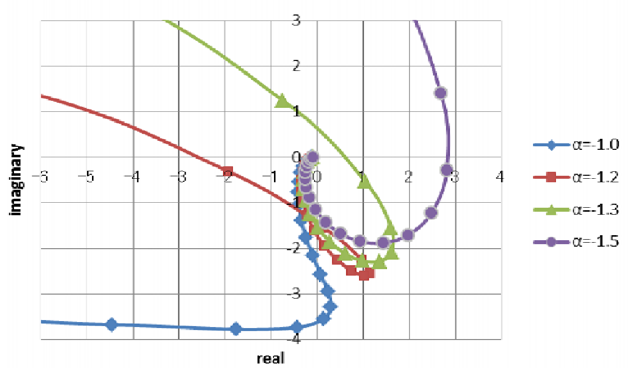

Fig. 6.39 Nyquist's trajectory by load's voltage sensitivity

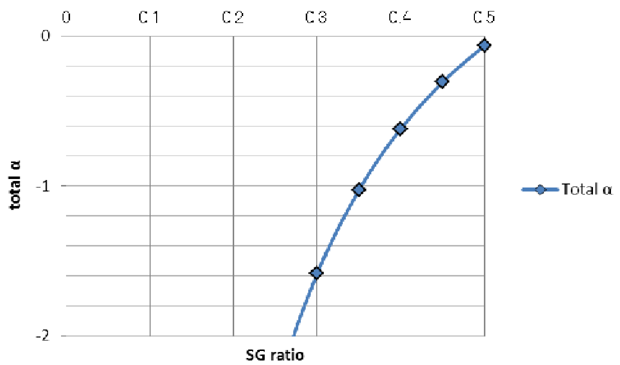

図 6.40 Voltage sensitivity of residual load by SG ratio

When α around -1.3 appears? α and β vary by branch impedance and capacitor amount. Assuming that (1) voltage sensitivity of load's active power α_L = 1 and that of RE's active power α_{PV} = 2, and assuming that (2) appearing residual load's voltage sensitivity at generator terminal (total α) is equal to residual load's sensitivity at load terminal where PV connects, result that (3) total α varies by SG ratio as shown in Fig. 6.40 is conducted. While the system is unstable at α is -1.3 or smaller in Nyquist's trajectory, the value is realized when SG ratio is smaller than 0.35.

Verification by simulation Theoretical analysis above is so rough that verification by simulation is needed. CRIEPI Y-method is used as tool, and generator is modeled minutely as Table 6.9.

Table 6.9 Generator constants in simulation

Xd	Xd'	Xd"	Xq	Xq'	Xq"	Td'	Td"	Tq'	Tq"
1.8	0.3	0.23	1.75	0.46	0.23	1.0	0.025	0.2	0.025
Xl	Ta	Sat. Vt= 0.5	0.8	1.0	1.1	1.2			
0.19	0.2	If = 0.5	0.819	1.114	1.387	1.767			

Static load case is simulated. At first, when both load and PV are constant impedance (that is, $\alpha_L = \beta_L = 2$, $\alpha_{PV} = \beta_{PV} = 2$), simulation result is shown in Fig. 6.41 by load voltage. Even in 5% SG ratio, the system is still stable.

Next, when load's active power only changed to constant current (that is, αL =1, $\beta_L = 2$, $\alpha_{PV} = \beta_{PV} = 2$), simulation result is shown in Fig. 6.42 by load voltage. Growing oscillation appears when SG ratio is smaller than 35% .

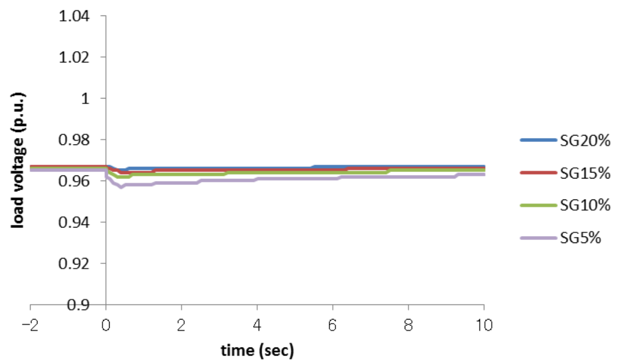

Fig. 6.41 Simulation (α_L=2, β_L=2, CZ-PV)

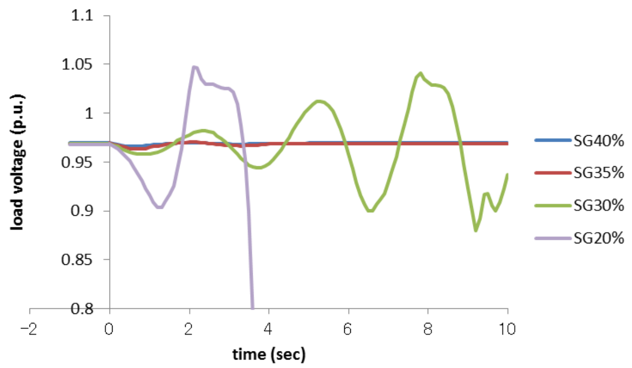

Fig. 6.42 Simulation (α_L=1, β_L=2, CZ-PV)

As dynamic load, mix of 50% induction motor 50% constant impedance is modeled. First, constant impedance PV ($\alpha_{PV} = \beta_{PV} = 2$) is assumed. Simulation result is ahown in Fig. 6.43. Growing oscillation occurs when SG ratio is smaller than 30% .

Next with 50% IM load, constant current PV ($\alpha_{PV} = \beta_{PV} = 1$) is assumed. Simulation result is shown in Fig. 6.44. Growing oscillation occurs when SG ratio smaller than 25% .

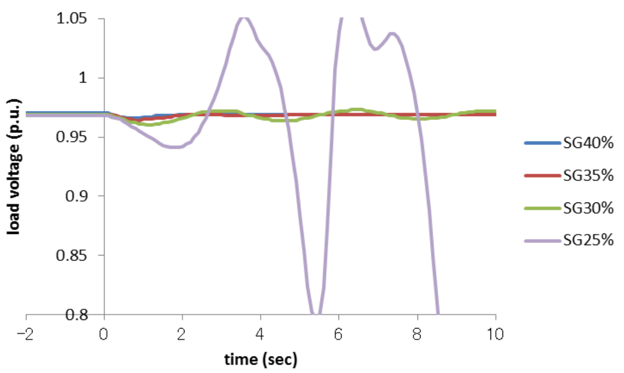

Fig. 6.43 Simulation (50%IM, CZ-PV)

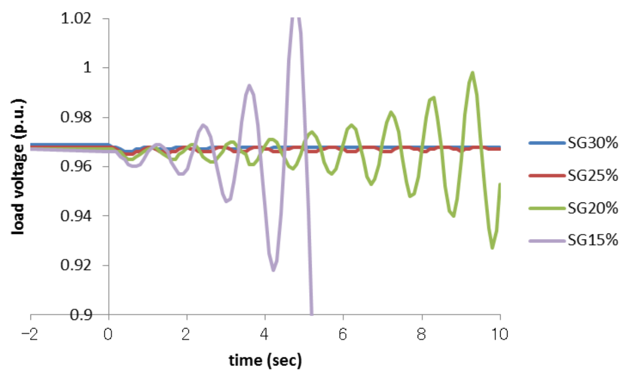

Fig. 6.44 シミュレーション(50%IM, CI-PV)

Further, with 50% IM load, constant power PV ($\alpha_{PV} = \beta_{PV} = 0$) is assumed. Simulation result is shown in Fig. 6.44by load voltage. Growing oscillation occurs when SG ratio is smaller than 45% .

Summing up case study above, Fig. 6.46 is obtained. In case of constant current load ($P \propto V^1$, $Q \propto V^2$), IM 50% load, oscillatory instability can occur. IM 50% load is nearly constant current load stationarily, but results slightly worse stability than constant current load, because of difference in reactive power's voltage sensitivity. In case of IM 50% load, constant current PV gives better atability. On the contrary, constant power PV gives worse stability.

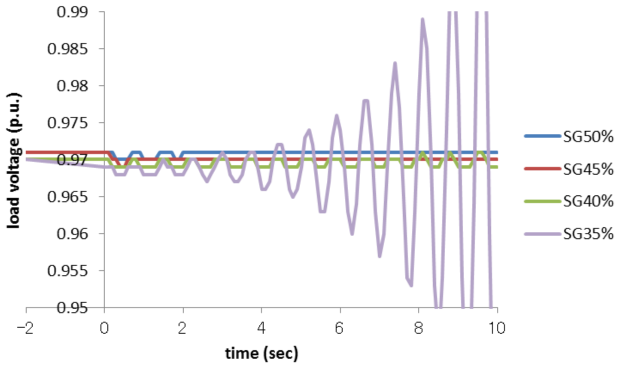

Fig. 6.45 Simulation (50%IM, CP-PV)

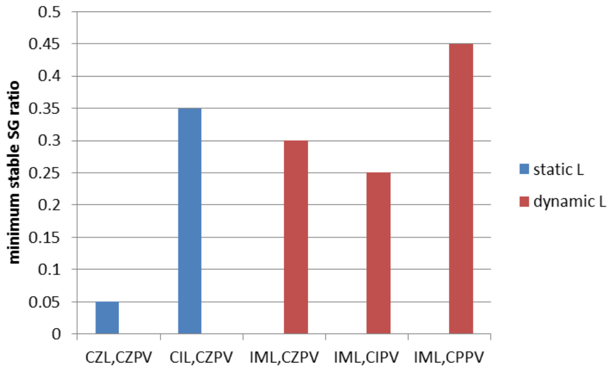

Fig. 6.46 Minimum stable SG ratio (part 1)

Instability by constant power RE In Fig. 6.45 oscillatory instability appears at low synchronous generator ratio when PV has constant power character. The mechanizm is explaines as follows. Induction motor accelerates after synchronous generator accelerates because of inertia. Therefore, induction motor slip is large ans internal resistance is small when synchronous generator is accelerating. Usually consumption power of load and PV complex is large in the situation. However, when impedance of synchronous generator seen from load and PV is large, operational condition belongs to lower half of P-V curve and consumption power of load and PV becomes amall. Low consumption power during generator acceleration means negative damping.

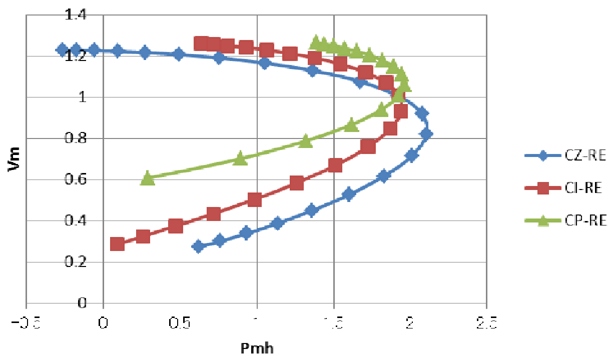

Fig. 6.47 P-V curves of load and PV

When synchronous generator ratio is 40%, P-V curves with constant impedance, constant current, and constant power RE are shown in Fig. 6.47. Certainly, equilibrium (almost 1.0 voltage) belongs to lower half. In analyses before, constant current or slightly nearer to constant power RE is favorable for power system stability. However, in islanded system with much RE, constant power RE causes oscillatory instability. As the phenomenon is local onearound synchronous generator's rotor, reasonable mitigation method does not exist. Thus, it is favorable to set RE voltage character within constant current.

Impact of excitation system design Oscillatory stability is much affected by excitation system design. In open loop gain, eq. (6.27), K6 never go negative. Therefore, AVR has a favorable effecf to return real part of K3 from negative to positive by adding positive K6 GAVR. That is, AVR improves oscillatory stability. However in case of AVR with large delay, gain's real part can so negative, so may spoil oscillatory stability[8].

On tha contrary, K2 can go negative. Therefore, ΔP type PSS adds K2 GPSS GAVR whose real part may negative onto K3, so oscillatory stability van be reduced.

Assume IM 50% load and constant impedance PV. ΔP type PSS case is alredy shown in Fig. 6.43. As to without PSS case, simulation result is shown in Fig. 6.48. Growing oscillation appear when SG ratio is smaller than 25%. Oscillatory stability is certainly spoiled by ΔP type PSS.

ΔP+Δω type PSS is examined. Its design is shown in Fig. 6.49. Input of Δω type is almost integral of ΔP type's input. Therefore, additioning Δω type without changing ΔP type as the figure, total PSS gain increases, and oscillatory stability will go worse.

Simulation result is shown in Fig. 6.50 by load voltage. Growing oscillation appears when at SG ratio is smaller than 35%.

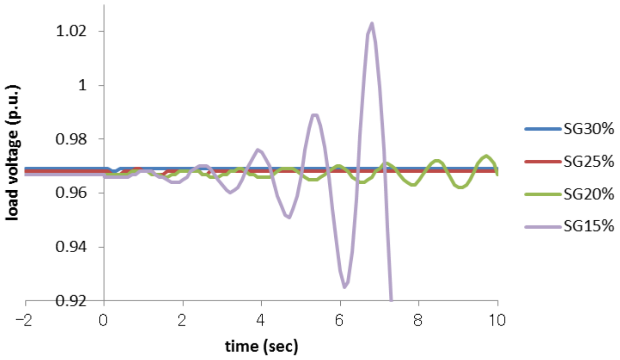

Fig. 6.48 Simulation (50%IM, CZ-PV, w/oPSS)

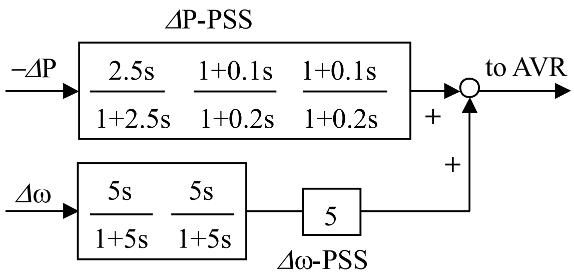

Fig. 6.49 Design of ΔP+Δω型 type PSS

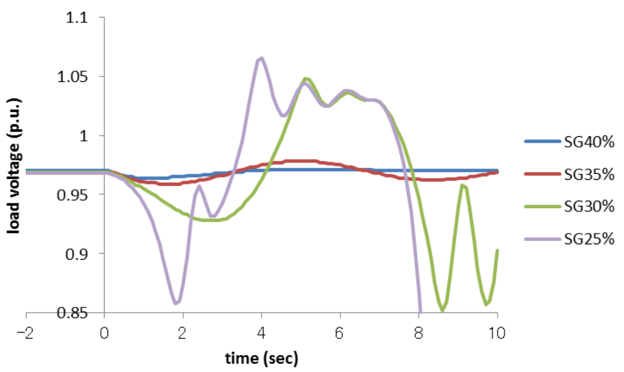

Fig. 6.50 Simulation (50%IM, CZ-PV, Δω-PSS)

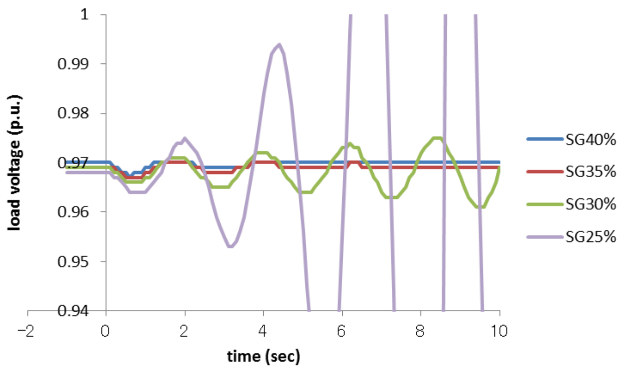

Fig. 6.51 Simulation (50%IM, CZ-PV, A-ISL)

It is already reported that RE's anti-islanding negatively impacts on usual angle oscillatory stability[9]. However, the same impact in islanded npower system case is not peported yet, so examined here. The result is shown in Fig. 6.51. In case of 50% IM load and constant impedance PV, growing oscillation appears when SG ratio is smaller than 35%.

Case study above is summed up in Fig. 6.52. Case without PSS is most stable, and ΔP+Δω type PSS shows the worst stability. RE's anti-islanding certainly reduce stability. However, impact of excitation system design and RE's anti-islanding is relatively smaller than that of

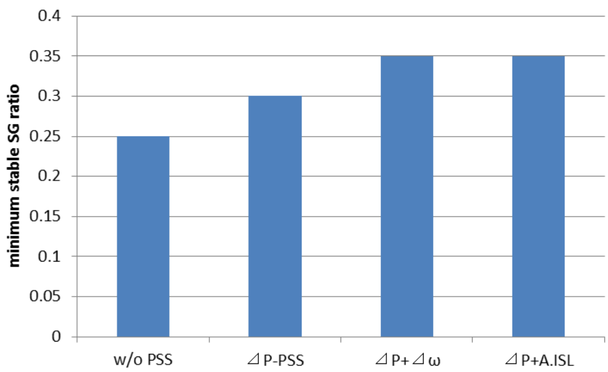

Fig. 6.52 Minimum stable SG ratio (part 2)

voltage sensitivity of active power.

Growing oscillation phenomenon is usually seen between two groups in loosely interconnected large system, and is not anticipated in tightly interconnected local islandednsystem. However, it was theoretically shown that another growing oscillation phenomenon can appear in local islanded system with highly integrated RE (here, PV). The phenomenon is regarded as a special case of usual oscillatory stability, and K_1, K_4, K_6 among de Mello's six coefficients go to zero.

The oscillatory instability appears by negative voltage sensitivity of residual load's active power seen from generater terminal when voltage sensitivity of load's active power is amaller than that of PV's active power. Also the instability go worse by PSS.

Therory is verified by similation.

References

(1) Maeda, Oigo, Komami, and Mizuno: "Story and Present Situation of Introducing PSS to Hokuriku EPCo.",Hokuriku EPCo. Technical Repository, No. 31, pp.39-58 (1990)

(2) S. Komami: "On the Importance of Power System Model Verification, Devils in Virtual Reality – Current and Future Subjects in Power System Simulation – ", IEEJ Journal, Vol. 132, No. 12, pp.820-823 (2012)

(3) W. G. Heffron, R. A. Phillips: "Effect of a modern amplidyne voltage regulator on underexcited operation of large turbine generators", Trans. AIEE Vol. 71, Pt. β, Aug. 1952, pp.692-697

(4) Y. Sekine: "Power System Analysis Theory", Denki-Shoin (1971)

(5) F. P. de Mello, C. Concordia: "Concepts of Synchronous Machines Stability as Affected by Excitation Control", IEEE Trans. PAS-88, Vol. 4, 316, 1969.

(6) S. Komami, S. Kimura, T. Komukai, and K. Koyanagi: "Effect of Load Characteristics on Dynamic Stability of Power System", IEEJ Trans. PE, Vol. 107-B, No. 7, pp.341-348 (1987)

(7) S. KOmami: "Dynamic Stability in Power System Receiving Power from Infinite Bus", IEEJ Annual Conference in PE, No. 30 (1990)

(8) Y. Yamagishi and S. Komami: "Power System Dynamic Stability Analysis Considering Dynamic Load and Distributed Generation", IEEJ Trans. PE, Vol. 126, No. 10, pp.977-984, (2006)

(9) S. Komami, T. Sakata, and S. Yamada: "Impact of RE's Anti-Islanding on Power System Oscillatory Stability", IEEJ Trans. PE, Vol. 136, No. 6, pp.557-568 (2016)

(10) E. W. Kimbark, "Power System Stability Ⅲ Synchronous Machines", Wiley, 1956

(11) K. Mizuo and S. Komami: "Parameter Identification Improvement of Dynamic Load Model in Power System", IEEJ Trans. PE, Vol. 132, No. 1, pp.71-76 (2012)

(12) Y. Yamagishi and S. Komami : "Practical Power System Aggregation Considering Dynamic Loads", IEEJ Trans. on PE, Vol. 128, No. 2, pp. 381-387 (2008)